arXiv:1412.8359v2 [cond-mat.mes-hall] 13 Apr 2015

Charge and spin transport in edge channels of a $\nu = 0$ quantum Hall system on the surface of topological insulators

Takahiro Morimoto,[1] Akira Furusaki,[1,2] and Naoto Nagaosa[2,3]

[1] *Condensed Matter Theory Laboratory, RIKEN, Wako, Saitama, 351-0198, Japan*
[2] *RIKEN Center for Emergent Matter Science (CEMS), Wako, Saitama, 351-0198, Japan*
[3] *Department of Applied Physics, The University of Tokyo, Tokyo, 113-8656, Japan*

(Dated: April 14, 2015)

Three-dimensional topological insulators of finite thickness can show the quantum Hall effect (QHE) at the filling factor $\nu = 0$ under an external magnetic field if there is a finite potential difference between the top and bottom surfaces. We calculate energy spectra of surface Weyl fermions in the $\nu = 0$ QHE and find that gapped edge states with helical spin structure are formed from Weyl fermions on the side surfaces under certain conditions. These edge channels account for the nonlocal charge transport in the $\nu = 0$ QHE which is observed in a recent experiment on $(Bi_{1-x}Sb_x)_2Te_3$ films. The edge channels also support spin transport due to the spin-momentum locking. We propose an experimental setup to observe various spintronics functions such as spin transport and spin conversion.

Introduction — The quantum Hall effect (QHE) is a representative topological quantum phenomenon where edge channels play an essential role in low-energy transport [1, 2]. The emergence of gapless edge channels is closely tied to nontrivial topology of gapped electronic states in the bulk, which is the property called bulk-edge correspondence. For topological insulators (TIs) [3, 4], the bulk-edge correspondence dictates that any surface of a three-dimensional (3D) TI with a nontrivial $\mathbb{Z}_2$ index has a single (or an odd number of) flavor(s) of Weyl fermions with spin-momentum locking. The surface Weyl fermions are predicted to give a variety of novel phenomena such as the quantized topological magneto-electric (ME) effect [5] and monopole-like magnetic field distribution induced by a point charge [6]. Another remarkable phenomenon is the quantized anomalous Hall effect *without* an external magnetic field [7–10]. By contrast, in an external magnetic field, a single flavor of Weyl fermions are expected to show a "half-integer" QHE with the Hall conductance $\sigma_{xy} = (n + \frac{1}{2})e^2/h$ $(n \in \mathbb{Z})$, which has a $\frac{1}{2}$-shift due to their nontrivial Berry phase, compared with the quantized Hall conductance of non-relativistic electrons, $\sigma_{xy} = ne^2/h$ $(n \in \mathbb{N})$.

However, the "half-integer" QHE is forbidden by the Nielsen-Ninomiya theorem [11], which dictates that there should be an even number of flavors of Weyl fermions in the first Brillouin zone, implying that the half-integer QHE is not observable in reality. For example, Weyl fermions in graphene have four flavors from spin and valley degrees of freedom, yielding $\sigma_{xy} = 4(n + \frac{1}{2})e^2/h$ [12]. As for a 3D (strong) TI, excitations at all surfaces have to be considered together. In a magnetic field applied perpendicular to the top and bottom surfaces of a 3D TI, Weyl fermions on the both surfaces contribute to σ_{xy}, yielding $\nu := \sigma_{xy}/(e^2/h) = n_T + n_B + 1$ with $n_T + \frac{1}{2}$ and $n_B + \frac{1}{2}$ coming from the top and bottom surfaces, respectively. The integers n_T and n_B are LL indices of the highest occupied LLs at the top and bottom surfaces. When the same number of LLs are filled at the top and bottom surfaces ($n_T = n_B$), the Hall conductivity is quantized at an odd integer [13]. However, the QHE of surface Weyl fermions with Hall plateaus at $\nu = 2, 3, 4, \ldots$ is experimentally observed in 3D HgTe [14]. More recent experiments on $(Bi_{1-x}Sb_x)_2Te_3$ films have reported plateaus at $\nu = 0$ and ± 1 as the gate voltage (Fermi energy) is changed [15, 16]. The appearance of $\nu = 0$ plateau violating the odd-integer rule indicates that the degeneracy between the top and bottom surfaces is lifted in $(Bi_{1-x}Sb_x)_2Te_3$ films [15, 16]. Moreover, a transport measurement on $(Bi_{1-x}Sb_x)_2Te_3$ films revealed the existence of nonlocal transport in the $\nu = 0$ QHE [24]. The nonlocal transport appears to conflict with the $\nu = 0$ QHE because of the absence of the chiral edge mode supporting the nonlocal transport.

In this paper, we study the $\nu = 0$ QHE (i.e., $n_T + n_B + 1 = 0$) of Weyl fermions on the surfaces of a 3D TI of finite thickness. Compared with the $\nu = 0$ QHE in graphene, which has been studied actively both experimentally [17–20] and theoretically [21, 22], the QHE in 3D TIs has the following unique features. First, the Weyl fermions on the TI surfaces are two-component spinors of real spin-$\frac{1}{2}$ degrees of freedom (as opposed to pseudo-spins in graphene), and the edge channels support both charge and spin transport. Second, in a magnetic field the Weyl fermions on the top and bottom surfaces (which are perpendicular to the field) form Landau levels (LLs), while those on the side surface (parallel to the magnetic field) are not directly affected by the field. However, one cannot consider independent 2D top and bottom surfaces of $\sigma_{xy} = \pm e^2/2h$ with edge channels. The side surface which connects the top and bottom surfaces must be taken into account when discussing the edge channels. The energy spectrum of the Weyl fermions on the side surface is discretized in a thin 3D TI, yielding well-defined edge channels under the condition of Eq. (4). These edge channels account for the

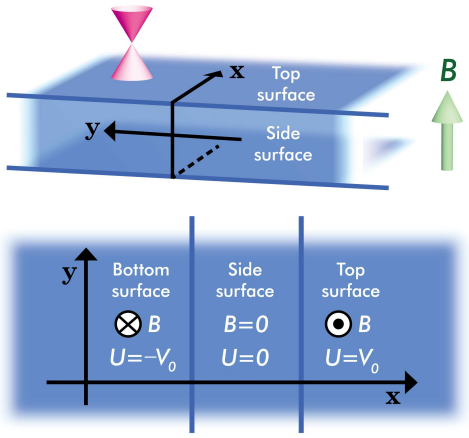

FIG. 1. Schematic picture of the two-dimensional (2D) model for the surface Weyl fermions of a topological insulator in a magnetic field. A 2D plane in the lower panel represents the top, bottom and side surfaces, where the strength of the magnetic field is $\pm B$ for $x > d$ and $x < -d$ and vanishing for $-d < x < d$.

nonlocal charge transport in the $\nu = 0$ QHE observed in the recent experiment [24]. Furthermore, since these edge channels are spin-momentum locked, the $\nu = 0$ QHE of TI thin films offers a new arena for various spintronics functions such as spin transport and spin conversion.

Model — We study quantum Hall states on the surfaces of a TI, treating the top, bottom, and side surfaces as an effective two-dimensional (2D) system as shown in Fig. 1. We will ignore the gapped bulk states. The top (bottom) surface is mapped onto the region $x > d$ ($x < -d$) with magnetic fields $+B\hat{\boldsymbol{z}}$ ($-B\hat{\boldsymbol{z}}$), while the side surface is mapped onto the region $-d \le x \le d$, where no magnetic field is applied; see the lower picture in Fig. 1. The effective Hamiltonian for the surface Weyl fermions is given by

$$H = v_F[-(p_x + eA_x)\sigma_y + (p_y + eA_y)\sigma_x] + U\sigma_0, \quad (1)$$

where v_F is the Fermi velocity, $\boldsymbol{p} = (p_x, p_y)$ is the momentum, and Pauli matrices $\boldsymbol{\sigma} = (\sigma_x, \sigma_y, \sigma_z)$ act on the spin degrees of freedom, and σ_0 is a 2×2 unit matrix. The vector potential $\boldsymbol{A} = (A_x, A_y)$ and the scalar potential U are functions of x,

$$\begin{aligned} &\boldsymbol{A}(x) = \big(0, -B(x+d)\big), && U(x) = -V_0, && (x < -d), \\ &\boldsymbol{A}(x) = (0,0), && U(x) = 0, && (|x| < d), \\ &\boldsymbol{A}(x) = \big(0, B(x-d)\big), && U(x) = V_0, && (x > d). \end{aligned} \quad (2)$$

We have introduced the potential difference between the top and bottom surfaces, $2V_0$. Since the 2D model is translationally invariant along the y direction under the Landau gauge, the momentum k_y is a good quantum number. The wave functions with wave number k_y

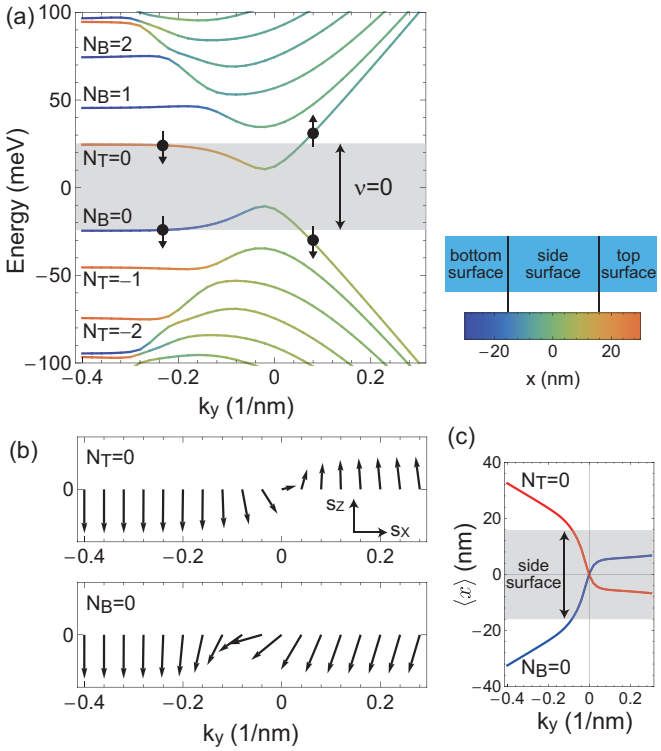

FIG. 2. Band structure of the surface Weyl fermions in the 2D model. (a) The energy levels of H in the Landau gauge [Eq. (1)] are plotted against the momentum k_y for $2d = 30\,\mathrm{nm}$, $B = 15\,\mathrm{T}$, $2V_0 = 50\,\mathrm{meV}$. Colors encode the expectation value of the position $\langle x\rangle$; the Landau levels on the top and bottom surfaces are depicted in red and blue in the region $k_y < 0$, while dispersive bands in green are edge channels on the side surface. LLs at the top (bottom) surface are labelled by indices N_T (N_B). (b) Spin textures in the (s_x, s_z)-plane and (c) expectation values $\langle x\rangle$ of the two bands connected to the $N_T = 0$ and $N_B = 0$ LLs. Edge channels ($k_y \gtrsim 0$) show the spin-momentum locking, while the $N = 0$ Landau levels on the top and bottom surfaces are spin polarized.

have a Gaussian form in x, with the expectation value $|\langle x\rangle| \simeq -k_y\ell^2$ for $k_y < 0$ and $\langle x\rangle \simeq 0$ for $k_y > 0$, where $\ell = \sqrt{\hbar/eB}$ is the magnetic length; see Fig. 2(c).

Edge channels — We show the band structure of the Hamiltonian [Eq. (1)] in Fig. 2(a). The bands are plotted as functions of k_y for the following parameters: $2d = 30\,\mathrm{nm}$, $B = 15\,\mathrm{T}$, $2V_0 = 50\,\mathrm{meV}$, and $v_F = 5\times10^5\,\mathrm{m/s}$ [23]. The flat bands at $k_y < 0$, shown in red and blue, are the LLs on the top and bottom surfaces, whose energies are given by

$$E_N = \mathrm{sgn}(N)\sqrt{|N|}\hbar\omega_c + U_0, \quad (3)$$

with the LL indices $N = N_T$ (N_B) and the scalar potential $U_0 = V_0$ ($-V_0$) for the top (bottom) surface, and the cyclotron frequency $\omega_c = v_F\sqrt{2eB/\hbar}$. Shown in green/yellow at $k_y \gtrsim 0$ are the energy bands of Weyl fermions on the side surface, which are separated by the

finite-thickness effects. The band structure in Fig. 2(a) can be naturally obtained by smoothly connecting LLs on the top and bottom surfaces to the discrete energy bands of Weyl fermions of the side surface. The $N_{T/B} = 0$ LLs on the top and bottom surfaces are separated by the energy difference $2V_0$. Thus, the $\nu = 0$ QHE is realized when the Fermi energy E_F is in the energy window $-V_0 < E_F < V_0$, because LLs are filled up to $N_T = -1$ and $N_B = 0$ LLs at top and bottom surfaces, respectively, and hence $\nu = n_T + n_B + 1 = 0$ with $n_T = -1$ and $n_B = 0$. In this case there is no chiral edge mode, as expected from the bulk-edge correspondence. However, transport through edge channels is still possible in the $\nu = 0$ QHE, under the conditions we discuss below.

Three parameters control the existence of edge channels in the $\nu = 0$ QHE: the energy difference of the Weyl points of the top and bottom surfaces $2V_0$, the cyclotron energy $\hbar\omega_c$, and the energy gap at $k_y = 0$ of the Weyl fermions on the side surface $\Delta_{\rm side} \simeq \hbar v_F/2d$. The edge channels in the $\nu = 0$ QHE can exist when

$$\Delta_{\rm side} < 2V_0 \leq \hbar\omega_c. \tag{4}$$

The left inequality implies that the two bands from the $N_{T/B} = 0$ LLs turn into helical edge channels on the side surface with energies in the $\nu = 0$ quantum Hall regime ($|E| < V_0$), whereas the right inequality assures that the $N_{T/B} = 0$ LLs are located in between the $N_T = -1$ and $N_B = +1$ LLs. The above conditions are satisfied by the parameters used in Fig. 2(a), which shows edge modes with a gap at $k_y = 0$. Furthermore, we find that, for the parameters in the experiment of $(Bi_{1-x}Sb_x)_2Te_3$ in Ref. [16], the above inequalities are satisfied with $2V_0 = 70\,\text{meV}$, $\hbar\omega_c = 70\,\text{meV}$, and $\Delta_{\rm side} \simeq 40\,\text{meV}$.

In Fig. 2(b) we show the expectation values of $(\langle s_x\rangle, \langle s_z\rangle)$ for the Bloch wave functions of the valence top band and the conduction bottom band, connected to the $N_B = 0$ and $N_T = 0$ LLs, respectively; we find $\langle s_y\rangle = 0$ for all bands. Note that, since we have rotated the side and bottom surfaces around the y axis by 90° and 180°, respectively, in our 2D model of TI surfaces (Fig. 1), the spins are also rotated accordingly. Thus the real spin operators $\boldsymbol{s}$ are written in terms of the Pauli matrices in the Hamiltonian [Eq. (1)] as

$$\frac{\boldsymbol{s}}{\hbar/2} = \begin{cases} (\sigma_x, \sigma_y, \sigma_z), & (x > d), \\ (-\sigma_z, \sigma_y, \sigma_x), & (-d < x < d), \\ (-\sigma_x, \sigma_y, -\sigma_z), & (x < -d). \end{cases} \tag{5}$$

The spins of the $N_{T/B} = 0$ LLs on the top and bottom surfaces are polarized, $(\langle s_x\rangle, \langle s_z\rangle) = (0, -\hbar/2)$ for $k_y < 0$. As k_y increases, the spin configuration crosses over to a helical spin structure of the edge channels on the side surface for $k_y \gtrsim 0$, where the spins of the two bands are polarized to the opposite directions because of the spin-momentum locking. This feature is similar to helical edge states of quantum spin Hall insulators, except for the presence of the gap at $k_y = 0$. We note that, when V_0 is negative, all the discussion above applies by replacing V_0 by $-V_0 = |V_0|$, except that $\langle s_x\rangle$ becomes $-\langle s_x\rangle$ in the spin texture. This is because the reflection $z \to -z$ changes the sign of V_0 and also $(s_x, s_y) \to (-s_x, -s_y)$.

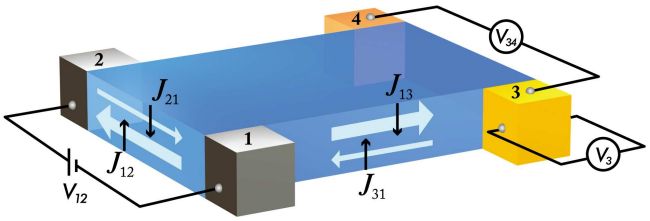

FIG. 3. A setup for the detection of charge and spin transport through edge channels. Applying a voltage between the electrodes 1 and 2 in the left induces charge and spin transport through the edge channels in the $\nu = 0$ quantum Hall state. The nonlocal charge transport is measured by the voltage V_{34} between the electrodes 3 and 4. The spin current is detected by the voltage V_3 between the two sides of the Pt electrode 3 via the inverse spin Hall effect.

Charge and Spin transport by edge channels — The edge channels on the side surface are responsible for the charge and spin transport, when the Fermi energy is in the range $\Delta_{\rm side} < |E_F| < V_0$. (Unlike in the quantum Hall insulators, however, the charge and spin conductances are not quantized because backscattering is allowed in these edge channels.) Here we propose an experimental setup consisting of a TI thin film with four electrodes to observe the charge/spin transport through edge channels; see Fig. 3. In the following we will discuss three characteristic transport phenomena: charge transport, spin transport, and spin conversion.

First, the edge channels should lead to nonlocal transport of charge. We predict that, when a voltage is applied and electric current flows between the electrodes 1 and 2, a finite voltage V_{34} between the electrodes 3 and 4 should be observed. Let us assume $V_0 < E_F < \Delta_{\rm side}$. The applied voltage induces net flow of up-spin electrons to the $+y$ direction and that of down-spin electrons to the $-y$ direction, according to Fig. 2. This results in the flow of electrons to the directions indicated by the thick arrows J_{12} and J_{13} in Fig. 3 (note that the electric current flows to the opposite directions), while the bulk transport is vanishing. The thin arrows represent the residual flow of electrons which were not absorbed by electrodes. The current J_{13} flows further along the right and rear side surfaces before reaching the electrode 2, yielding a finite voltage V_{34} between the electrodes 3 and 4. The nonlocal transport in the $\nu = 0$ quantum Hall regime has been actually observed in experiments of $(Bi_{1-x}Sb_x)_2Te_3$ films [24].

Second, the edge channels support spin transport in

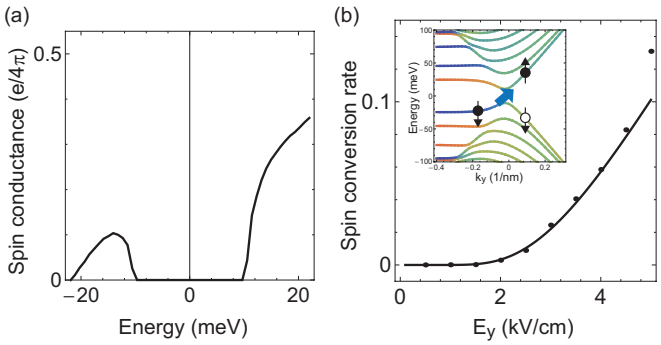

FIG. 4. (a) Spin conductance as a function of the Fermi energy. Spin conductance is finite in the $\nu = 0$ quantum Hall state when the Fermi level is in the edge channels. (b) Spin conversion rate plotted against electric fields E_y. Dots represent the spin conversion rate obtained from numerical solutions of the time-dependent Schrödinger equation, while the solid curve is given by the Zener tunneling formula [Eq. (9)]. Results in both panels are obtained for the same parameters used in Fig. 2(a).

addition to the charge transport. As we have discussed above, the applied voltage V_{12} produces the circulating spin polarized electronic current through the edge channels, as shown in Fig. 3. We predict that the nonvanishing spin current should yield a finite voltage V_3 between the two sides of the electrode 3 if it is made of a material with strong spin-orbit coupling such as Pt. The spin current J_{13} diffusing into the electrode 3 produces a flow of down-spin electrons moving perpendicular to the side surface. This spin current will generate the voltage V_3 through the inverse spin Hall effect (ISHE) [25] in the electrode 3. The voltage V_3 is determined by the spin conductance of the edge channels, the diffusion rate across the interface of the electrode 3, and the efficiency of the ISHE. The (linear) spin conductance G_{s_z} is calculated in the ballistic regime as

$$G_{s_z} = \sum_i \int \langle s_z \rangle_{i,k_y} |v_{i,k_y}| \left(-\frac{e}{2}\right) \frac{df(\epsilon_{i,k_y})}{d\epsilon} dk_y, \qquad (6)$$

where $f(\epsilon)$ is the Fermi distribution function, and $\langle s_z \rangle_{i,k_y}$ is the expectation value of s_z for the Bloch wave function ψ_{i,k_y} of the ith band with the momentum k_y and the energy ϵ_{i,k_y}. The group velocity v_{i,k_y} along the y direction is given by $v_{i,k_y} = \hbar^{-1} d\epsilon_{i,k_y}/dk_y$. In deriving Eq. (6) we have assumed that the applied voltage V shifts the Fermi energy of the right-going (left-going) electrons by $V/2$ ($-V/2$) in the ballistic regime. In Fig. 4(a) we show the spin conductance at zero temperature which is calculated as a function of E_F with the parameters used in Fig. 2(a). The spin conductance G_{s_z} is non-vanishing when the Fermi energy lies in the edge channels. The asymmetry of the spin conductance in E_F reflects the different spin configurations of the two bands connected to the $N_{T/B} = 0$ LLs shown in Fig. 2(a).

Finally, we discuss spin conversion due to interband transitions that occur at the side surface in the nonequilibrium regime. We assume that the Fermi energy is within the gap $\Delta_{\rm side}$. When an electric field is applied, by external gate electrodes, to the sample in the direction from the electrode 2 to the electrode 1, electrons in the $N_B = 0$ band are driven by the electric field and undergo Zener tunneling into the $N_T = 0$ band across the energy gap around $k_y = 0$ as shown in the inset of Fig. 4(b), where k_y is along the direction from the electrode 1 to the electrode 2. In this process, a pair of a spin-up electron in the $N_T = 0$ band and a spin-down hole in the $N_B = 0$ band is created. Thus the Zener tunneling in the edge channels gives rise to spin conversion and spin accumulation at the side surface between the electrodes 1 and 2. In order to quantify the spin conversion, we study the time-evolution of a wave packet driven by the electric field E_y along the y direction for the time period $t_f = \hbar(k_y^f - k_y^i)/eE_y$, from the initial state $\psi(t=0) = \psi_{N_B=0,k_y^i}$ in the $N_B = 0$ band with the momentum $k_y^i = -0.2$ nm^{-1} to the final state $\psi(t = t_f)$ with the momentum $k_y^f = 0.2$ nm^{-1}. To this end, we numerically solve the time-dependent Schrödinger equation,

$$i\hbar\partial_t \psi(t) = (H + v_F e E_y t \sigma_x)\psi(t), \qquad (7)$$

and compute the spin conversion rate $P(E_y)$

$$P(E_y) = \langle s_z \rangle_{t=t_f} - \langle s_z \rangle_{N_B=0,k_y^f}, \qquad (8)$$

where $\langle s_z \rangle_{t=t_f}$ is the expectation value of s_z in the final state $\psi(t_f)$. The obtained spin conversion rate in Fig. 4(b) shows a nonlinear response to E_y, which is consistent with the Zener tunneling formula,

$$P(E_y) \propto \exp\left(-\frac{2\pi}{\hbar}\frac{\Delta_{\rm side}^2}{2v_F e E_y}\right), \qquad (9)$$

for the two-band system of the $N_T = 0$ and $N_B = 0$ bands with the energy gap $\Delta_{\rm side} \simeq v_F\hbar/2d$.

Summary — We have studied charge and spin transport in the $\nu = 0$ quantum Hall system of surface Weyl fermions of 3D TIs. The charge and spin currents are carried by the edge channels formed on the side surfaces of TIs. A unique feature of the QHE in TIs is that the top and bottom surfaces, where LLs are formed, are connected by side surfaces, where Weyl fermions form edge channels, as contrasted to conventional quantum Hall bilayers and the $\nu = 0$ QHE in graphene. In the proposed spin transport experiment, the voltage V_3 is expected to be on the order of 10 nV as measured in an experiment of ISHE [26]. The spin conversion rate is typically $0.1 \sim 1\,\%$ under the electric field $E_y \simeq 1$ kV/cm, when electric current of a few mA flows in a 1 mm sample [16]. We expect

that the spin accumulation can be detected by Kerr rotation of the order of 10 μrad at the edge of TI thin films [27].

The authors are grateful for insightful discussions with M. Kawasaki and Y. Tokura. This work was supported by Grant-in-Aids for Scientific Research (No. 24224009 and No. 24540338) from the Ministry of Education, Culture, Sports, Science and Technology (MEXT) of Japan and from Japan Society for the Promotion of Science.

[1] *The Quantum Hall Effect*, edited by R. E. Prange and S. M. Girvin (Springer-Verlag, New York, 1987).
[2] *Perspectives in Quantum Hall Effects*, edited by S. Das Sarma and A. Pinczuk (Wiley, New York, 1997).
[3] M. Z. Hasan and C. L. Kane, Rev. Mod. Phys. **82**, 3045 (2010).
[4] X.-L. Qi and S.-C. Zhang, Rev. Mod. Phys. **83**, 1057 (2011).
[5] X.-L. Qi, T. L. Hughes, and S.-C. Zhang, Phys. Rev. B **78**, 195424 (2008).
[6] X.-L. Qi, R. Li, J. Zang, S.-C. Zhang, Science **323**, 1184 (2009).
[7] F. D. M. Haldane, Phys. Rev. Lett. **61**, 2015 (1988).
[8] M. Onoda and N. Nagaosa, Phys. Rev. Lett. **90**, 206601 (2003).
[9] R. Yu, W. Zhang, H.-J. Zhang, S.-C. Zhang, X. Dai, and Z. Fang, Science **329**, 61 (2010).
[10] C.-Z. Chang et al., Science **340**, 167 (2013).
[11] H. B. Nielsen and M. Ninomiya, Phys. Lett. **B105**, 219 (1981).
[12] A. H. Castro Neto et al., Rev. Mod. Phys. **81**, 109 (2009).
[13] D.-H. Lee, Phys. Rev. Lett. **103**, 196804 (2009).
[14] C. Brüne, C. X. Liu, E. G. Novik, E. M. Hankiewicz, H. Buhmann, Y. L. Chen, X. L. Qi, Z. X. Shen, S. C. Zhang, and L. W. Molenkamp Phys. Rev. Lett. **106**, 126803 (2011).
[15] Y. Xu et al., Nat. Phys. **10**, 956 (2014).
[16] R. Yoshimi et al., arXiv:1409.3326 (to appear in Nat. Commun.).
[17] D. A. Abanin et al., Phys. Rev. Lett. **98**, 196806 (2007).
[18] J. G. Checkelsky, L. Li, and N. P. Ong, Phys. Rev. Lett. **100**, 206801 (2008).
[19] A. J. M. Giesbers et al., Phys. Rev. B **80**, 201403(R) (2009).
[20] Y. Zhao, P. Cadden-Zimansky, F. Ghahari, and P. Kim, Phys. Rev. Lett. **108**, 106804 (2012).
[21] D. A. Abanin, P. A. Lee, and L. S. Levitov, Phys. Rev. Lett. **96**, 176803 (2006).
[22] S. Das Sarma and K. Yang, Solid State Commun. **149**, 1502 (2009).
[23] The energy levels calculated for another set of parameters ($2d = 8\,\mathrm{nm}$, $B = 14\,\mathrm{T}$, $2V_0 = 70\,\mathrm{meV}$) taken from Ref. [16] are shown in supplemental material.
[24] R. Yoshimi, K. Yoshida, and Y. Tokura, unpublished.
[25] E. Saitoh, M. Ueda, H. Miyajima, and G. Tatara, Appl. Phys. Lett. **88**, 182509 (2006).
[26] Y. Omori, F. Auvray, T. Wakamura, Y. Niimi, A. Fert, and Y. Otani, Appl. Phys. Lett. **104**, 242415 (2014).
[27] Y. K. Kato, R. C. Myers, A. C. Gossard, D. D. Awschalom, Science **306**, 1910 (2004).

Supplemental material for "Charge and spin transport in edge channels of a $\nu = 0$ quantum Hall system on the surface of topological insulators"

LLs in top and bottom surfaces

Far from the side surface, we have well-defined Landau levels (LLs) at the top and bottom surfaces. In this region, the Hamiltonian [Eq. (1)] reduces to

$$H_{k_y} = v_F[-p_x\sigma_y + (\hbar k_y \pm eBx)\sigma_x] \pm V_0\sigma_0, \tag{S1}$$

where k_y is the momentum along the y direction and we choose the sign $\pm$ for the top and bottom surfaces. We note that we replaced the gauge potential with $A_y = \pm Bx$ for simplicity. We assume $B > 0$. The energy and wavefunction of LLs for the above Hamiltonian are written as follows. For the top surface, the LLs are written as

$$\begin{aligned} E_{N_T,k_y} &= \mathrm{sgn}(N_T)\sqrt{|N_T|}\hbar\omega_c + V_0, \\ \psi_{N_T,k_y}(x) &= \begin{pmatrix} \mathrm{sgn}(N_T)\phi_{|N_T|-1}\left(\frac{x-x_0(k_y)}{\ell}\right) \\ \phi_{|N_T|}\left(\frac{x-x_0(k_y)}{\ell}\right) \end{pmatrix}, \\ x_0(k_y) &= -\ell^2 k_y, \end{aligned} \tag{S2}$$

with

$$\mathrm{sgn}(n) = \begin{cases} +1, & (n > 0) \\ 0, & (n = 0) \\ -1, & (n < 0) \end{cases} \tag{S3}$$

where N_T is the Landau index at the top surface, ϕ_n is the wavefunction of conventional Landau levels with $\phi_{-1} = 0$, the cyclotron energy $\hbar\omega_c$ and the magnetic length ℓ are

$$\hbar\omega_c = v_F\sqrt{2\hbar eB}, \qquad \ell = \sqrt{\frac{\hbar}{eB}}. \tag{S4}$$

For the bottom surface, the LLs are written as

$$\begin{aligned} E_{N_B,k_y} &= \mathrm{sgn}(N_B)\sqrt{|N_B|}\hbar\omega_c - V_0, \\ \psi_{N_B,k_y}(x) &= \begin{pmatrix} \phi_{|N_B|}\left(\frac{x-x_0(k_y)}{\ell}\right) \\ \mathrm{sgn}(N_B)\phi_{|N_B|-1}\left(\frac{x-x_0(k_y)}{\ell}\right) \end{pmatrix}, \\ x_0(k_y) &= \ell^2 k_y. \end{aligned} \tag{S5}$$

where N_B is the Landau index at the bottom surface.

Band structure with parameters in an experiment of TI thin films

We show the band structure of the Hamiltonian [Eq. (1)] using the parameters in experiments by Yoshimi et al. [S1]: $2d = 8\,\mathrm{nm}$, $B = 15\,\mathrm{T}$, $2V_0 = 70\,\mathrm{meV}$, and $v_F = 5 \times 10^5\,\mathrm{m/s}$. The band structure is plotted as a function of k_y in Fig. S1(a). We find that $N_B = 0$ and $N_T = -1$ LLs and $N_B = 1$ and $N_T = 0$ LLs are almost degenerate. Edge channels appear in the $\nu = 0$ quantum Hall system (QHS) in the energy window $-V_0 < E_F < V_0$. The condition for the presence of edge channels [Eq. (4)] are satisfied with $\Delta_{\mathrm{side}} \simeq 40\mathrm{meV} < 2V_0$. This indicates that nonlocal transport observed in Ref. [S2] originates from the edge channels in the $\nu = 0$ QHS. The spin expectations values in Fig. S1(b) show that edge channels are spin-momentum locked and the $N = 0$ LLs are spin-polarized. Thus observations of the spin transport phenomena proposed in this paper are experimentally feasible in available topological thin films with the experimental setups in Fig. 3.

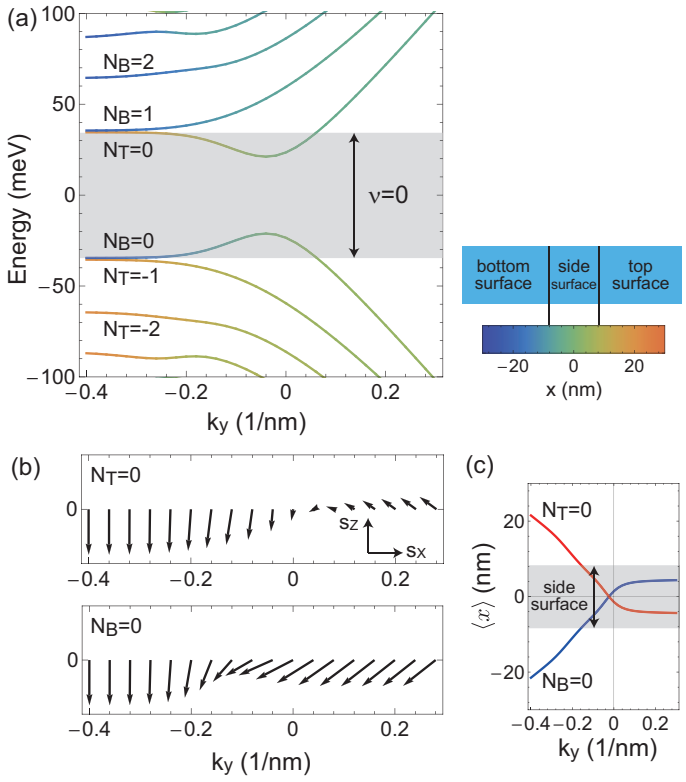

FIG. S1. Band structure of the surface Weyl fermions in the 2D model. (a) The energy levels of H in Eq. (1) are plotted against the momentum k_y for $2d = 8\,\mathrm{nm}$, $B = 15\,\mathrm{T}$, $2V_0 = 70\,\mathrm{meV}$. Colors encode the expectation value of the position $\langle x\rangle$; the Landau levels on the top and bottom surfaces are depicted in red and blue in the region $k_y < 0$, while linear bands in green are edge channels on the side surface. LLs at the top (bottom) surface are labelled by indices N_T (N_B). (b) Spin textures in the (s_x, s_z)-plane and (c) expectation values $\langle x\rangle$ of the two bands connected to the $N_T = 0$ and $N_B = 0$ LLs. Edge channels ($k_y \gtrsim 0$) show the spin-momentum locking, while the $N = 0$ Landau levels on the top and bottom surfaces are spin polarized.

Estimates of the parameters controlling presence or absence of the edge channels are given for $v_F = 5 \times 10^5\,\mathrm{m/s}$ as follows. The cyclotron energy $\hbar\omega_c$ is given by

$$\hbar\omega_c \simeq 18\sqrt{B(\mathrm{T})}\,\mathrm{meV}. \tag{S6}$$

The gap of the Weyl fermions at the side surface due to the finite size effect can be roughly estimated as

$$\Delta_{\mathrm{side}} \simeq \frac{\hbar v_F}{2d} \simeq \frac{320}{2d(\mathrm{nm})}\mathrm{meV}. \tag{S7}$$

[S1] R. Yoshimi et al., arXiv:1409.3326 (unpublished).
[S2] R. Yoshimi, K. Yoshida, and Y. Tokura, unpublished.